Scaling of heat transfer in gas–gas injector combustor*

Wang Xiao-Wei(汪小卫), Cai Guo-Biao(蔡国飙)†, and Gao Yu-Shan(高玉闪)

School of Astronautics, Beihang University, Beijing 100191, *China*

(Received 16 December 2010; revised manuscript received 11 January 2011)

The scaling of heat transfer in gas–gas injector combustor is investigated theoretically, numerically and experimentally based on the previous study on the scaling of gas–gas combustion flowfield. The similarity condition of the gas–gas injector combustor heat transfer is obtained by conducting a formulation analysis of the boundary layer Navier–Stokes equations and a dimensional analysis of the corresponding heat transfer phenomenon. Then, a practicable engineering scaling criterion of the gas–gas injector combustor heat transfer is put forward. The criterion implies that when the similarity conditions of inner flowfield are satisfied, the size and the pressure of gas–gas combustion chamber can be changed, while the heat transfer can still be qualitatively similar to the distribution trend and quantitatively correlates well with the size and pressure as $q \propto p_{\rm c}^{0.8} d_{\rm t}^{-0.2}$. Based on the criterion, single-element injector chambers with different geometric sizes and at different chamber pressures ranging from 1 MPa to 20 MPa are numerically simulated. A single-element injector chamber is designed and hot-fire tested at seven chamber pressures from 0.92 MPa to 6.1 MPa. The inner wall heat flux are obtained and analysed. The numerical and experimental results both verified the scaling criterion in gas–gas injector combustion chambers under different chamber pressures and geometries.

Keywords: similarity, heat transfer, gas–gas combustion, simulation, experiment

PACS: 47.70.–n, 44.90.+c, 47.27.te **DOI:** 10.1088/1674-1056/20/6/064701

1. Introduction

Scaling of combustion devices for liquid propellant rocket engines (LPREs) has been a subject of considerable difficulty and controversy since the advent of rocketry. Nevertheless, the use of scaling techniques is invaluable. The cost and the cycle can be sharply reduced by using subscale devices at low pressure (model) to develop full-scale ones (prototype).[1−5] The first formal liquid rocket scaling research was conducted by Penner more than 50 years ago,[1,2] but the studies have made no progress since then, owing to some historical reasons. However, in the current era it has been picked up by designers because of the higher requirements for performance and significant reduction in financing.[3−5]

The full flow stage combustion (FFSC) cycle engine is preferable because of its high performance and high reliability.[6] Gas–gas combustion technology is a key technology for this kind of engine. The FFSC nominal gas–gas injector main thrust chamber was designed at a chamber pressure of above 20 MPa and mass flowrate of above 450 kg/s. Also, gas–gas injectors have been widely used on other engines and combustion devices.[7,8] Thus it will be very valuable if a feasible scaling technique can be applied to the development of gas–gas injector chambers.

The key issue of the scaling technique is to ensure similarity of the phenomena between the model and prototype. The spray combustion process is composed of injection, atomization, vaporization, mixing and reaction. Because of its complexity and the strongly coupled relationships between them, scaling of the spray reacting flows with complete similarity is found to be impossible in practice. Thus, scaling of combustion devices for LPREs has not been fully developed yet. Nevertheless, the gas–gas combustion process only involves injection, mixing and reaction. The characteristics of the gas–gas injector chamber indicate a possibility of guaranteeing the similarity between the model and prototype on the whole.

The scaling technique of liquid rocket engine combustion devices was generally investigated and reviewed in Refs. [3]–[5], while scaling of gas–gas combustion combustor was not mentioned. Although a lot of studies have been carried out up to now on gas–gas injector,[8−29] the scaling of gas–gas combustor, unfortunately, is just starting. Wang[27] has conducted the research on scaling of gas–gas cold mixing flow utilizing the formulation analysis of the

*Project supported by the National High Technology Research and Development Program of China (Grant No. 2008AA7023) and the Innovation Foundation of Beihang University for Ph. D. Graduates (Grant No. 430569).

†Corresponding author. E-mail: cgb@buaa.edu.cn

© 2011 Chinese Physical Society and IOP Publishing Ltd

three-dimensional (3D) Navier–Stokes equations for a gaseous multi-component mixing flow and applying dimensional analysis on the gas–gas mixing phenomena. The scaling criterion was obtained and validated using the corresponding numerical simulation. Based on this cold flow research, Cai and Wang[28,29] successively studied the scaling of gas–gas combustion flowfield in single-element and multi-element gas–gas injector combustors. The scaling criterion also was validated using the corresponding numerical and experimental results. The scaling criterion of the gas–gas combustion flowfield obtained is as follows: a) similarity between the geometries of the injector and the chamber; b) identical propellants; c) constant injection velocities and propellant temperatures; d) nonslip and similar species wall boundary; e) flow in laminar or sufficient turbulence condition.

Although the above researches have revealed the scaling technology of the gas–gas combustion flowfield, it cannot be directly used in the engineering development applications of LPREs, because the combustion performance and heat transfer are always the objectives with which the engineering designers are concerned.[3−8,13−16] This paper just focuses on the scaling technology of heat transfer in gas–gas injector combustor. Another scaling criterion, namely, how to use low-pressure small-size model engine heat flux data to substitute for, or extend to high pressure large-size prototype engine, will be figured out. The cost and the development cycle can be significantly reduced and the potential danger of the devices operated in high pressure condition also can be avoided by using this criterion.

References [27]–[29] mainly focused on the similarity of main flow, ignoring the thin boundary layer. However, on the basis of similarity of the main flow, the scaling of heat transfer totally depends on the similarity of the boundary layer flow. Thus, the formulation analysis of the boundary layer equations and dimensional analysis of the boundary heat transfer phenomena in the gas–gas combustion chamber will be carried out in this paper to reveal the similarity condition of heat transfer. Then an engineering practicable scaling criterion will be put forward by further analysis of the similarity condition and successively validated by the numerical and experimental studies.

2. Formulation analysis

2.1. The boundary layer equations and monodromy condition

The Mach number in the combustion chamber always is small and the gravity force can be neglected. Assuming that there is no chemical reaction in the boundary layer and the boundary layer flow is two-dimensional (2D) to avoid unnecessary narration and facilitate the analysis, the dimensionless 2D equations governing gaseous boundary layer are given as follows:

$$\frac{\partial}{\partial x_j^*}\left(\rho^* u_j^*\right) = 0, \tag{1}$$

$$u^*\frac{\partial u^*}{\partial x^*} + v^*\frac{\partial u^*}{\partial y^*} = -Eu\frac{\partial p^*}{\partial x^*} + \frac{1}{Re}\frac{\partial^2 u^*}{\partial y^{*2}}, \tag{2}$$

$$u^*\frac{\partial T^*}{\partial x^*} + v^*\frac{\partial T^*}{\partial y^*} = Pe\frac{\partial^2 T^*}{\partial y^{*2}}, \tag{3}$$

where $Eu = p_\infty/\rho_\infty U_\infty^2$, $Re = \rho_\infty U_\infty L_\infty/\mu_\infty$, $Pe = a_\infty/L_\infty U_\infty = Pr\ Re$.

Constancy of all dimensionless groups for all processes between different combustion chambers ensures that the processes are strictly similar; they are summarized as follows: $Eu_1 = Eu_2$, $Re_1 = Re_2$, $Pr_1 = Pr_2$. The same results will be obtained, if using three-dimensional (3D) equations.

The similarity theory indicates that similarity between phenomena of the same type still requires similarity between their monodromy conditions. Here the conditions are given as follows:

(i) Geometric condition: geometric similarity.

(ii) Outer boundary condition of the boundary layer:

a) The velocity distribution in the mainflow on the outer boundary: $u_1 = u_2 = $ idem;

b) The temperature distribution in the mainflow on the outer boundary: $T_1 = T_2 = $ idem;

c) The species distribution in the mainflow on the outer boundary: $Y_1 = Y_2 = $ idem.

(iii) Wall boundary conditions:

a) Velocity boundary conditions: non-slip condition: $\partial v/\partial n = 0$;

b) Wall species boundary conditions: non-existence of or similar wall species boundary conditions.

2.2. Similarity criterion analysis

1) Eu

The Eu indicates the effects of surface forces. It is always important for studying the phenomena of water hammer and cavitation. In this study, it is not a main factor.[30] Additionally, $Eu = p_\infty/\rho_\infty U_\infty^2 = RT_\infty/U_\infty^2$, RT_∞ and U_∞ both are constant when main flowfields are similar. Thus, the Eu is easy to keep unchanged here.

2) Pr

The Pr belongs to the basic property parameters and must be ensured to be constant. When identical gaseous propellants are used, the Pr is kept constant.

3) Re

The Re is the ratio of inertial force to viscous force in the unit volume. It is an important parameter indicating the state of the motion and has been discussed in detail in Refs. [27]–[29]. If the flow is in a sufficient turbulence condition, the Re of the main flow of the model and prototype are not required to be the same due to the self-similar characteristics.

Also, in a rocket engine combustor, the boundary layer flow is always in turbulence condition. However, the boundary layer flow is different from the main flow. There are some different flow regions in the turbulence boundary layer, mainly including the viscous sublayer, transition sublayer and the turbulence sublayer.[31] In the inner viscous sublayer, the viscous force plays a dominant role. In the transition sublayer, viscous force and inertial force are roughly in the same order, while in the turbulence sublayer, inertial force becomes dominant. In the boundary layer, at least, the thickness of each sublayer and flowfield structure in the transition sublayer totally depend on the value of Re, which means different Re will produce different flow structures in the boundary layer. There is no self-similar characteristics for the boundary layer. The Re must be required to be constant for similarity of boundary layer flow.

4) Monodromy condition analysis

Similarity of the physical geometry is very easy to ensure. When the main flowfield is similar, the outer boundary conditions are automatically satisfied. Generally, the wall non-slip and similar species boundary conditions can be covered naturally in a regeneratively-cooled chamber. The wall species boundary conditions are assumed to be similar if there exist any conditions of this kind.

3. Dimensional analysis

Dimensional analysis is another theoretical method which can effectively serve the experimental studies. This method has wider applicability,[29,32] unfortunately, its application to the phenomena in LPREs is less documented by now. Without considering the reaction in the boundary layer, the parameters related to the heat transfer phenomenon in an LPRE include: velocity u, temperature T, diameter D, pressure p, fluid property parameters (density ρ, viscosity μ, specific heat C_p and thermal conductivity λ).

The specific monodromy conditions determine the unique solutions of the same kind of physical phenomena. When main flowfield has been identified, the pressure p in boundary layer also has been identified as the same as the main flow.[31] And the high temperature gas in the combustor can be treated as an ideal gas, thus the density and temperature become dependent on each other. Therefore, the independent parameters related to the heat transfer phenomenon in an LPRE can be obtained: u, D, ρ, μ, λ, and C_p. The heat transfer coefficient h is chosen as the research object here.

The basic units contained in these parameters are L (length), T (time), M (mass), and Θ (temperature) and u, D, ρ, and C_p are chosen as the basic parameters. As a result, for the application of the π theorem, three dimensionless parameters are introduced as follows:

$$\pi_1 = \frac{hD}{\lambda} = Nu, \quad \pi_2 = \frac{\rho u D}{\mu} = Re, \quad \pi_3 = \frac{\mu C_\mathrm{p}}{\lambda} = Pr.$$

Thus the following expression can be obtained:

$$Nu = f(Re, Pr). \tag{4}$$

Equation (4) indicates that the heat transfer will be similar as long as Re and Pr are kept constant. This result is the same as that of the formulation analysis.

Theoretical analysis shows that Re needs to be kept unchanged to ensure the similarity of heat transfer in the gas–gas injector combustor. This result can lead to a prefect scaling technology in which heat flux is independent of pressure and is inversely proportional to combustor size. However, this good quantitatively scaling relationship cannot always be achieved easily because it is hard to keep Re unchanged in practical engineering application. The related analysis will be carried out in detail in the following discussions.

4. Scaling criterion analysis

4.1. Scaling method analysis

If the main flowfields are similar, the temperature and property parameters will maintain constant and

then in the high temperature combustion chamber, $Re = \rho uD/\mu \propto \rho uD \propto puD$. Because in an LPRE combustor, the main flow velocity u is only related to the ratio of local section area to the throat section area (i.e. $u \sim f(A/A_t)$). Because the geometries must be similar, the velocity u becomes unchanged. Thus, $Re \propto pD$ can be deduced, namely the pressure must be inversely proportional to the size to keep Re constant in the scaling method. However, this scaling method becomes impractical. If low pressure hot tests are employed to simulate the high-pressure ones, impractical larger size combustion chambers will be needed, which cannot exhibit the value of the scaling technology.

Different Re produce different Nu. Because local normal boundary layer flow structures become dissimilar (i.e. $Nu_1 \neq Nu_2$), the quantitative scaling method of heat flux does not exist when Re are different. However, similarity of the main combustion flowfield is independent of Re for the sufficient turbulent flow in LPREs[27−29] and the wall boundary conditions always are satisfied here, which means that the inner and outer boundary conditions of similarity of boundary layer flowfield can both be satisfied regardless of Re. Thus, though different Re can produce local quantitatively dissimilar heat transfer and boundary layer flow structure, it still cannot avoid the existence of the qualitative similar heat transfer distribution on the combustor wall. Therefore, the qualitatively similarity of heat transfer distribution along with the wall always exists as long as the main flowfields are similar. Even though qualitative similarity of heat flux distribution can be easily obtained, the quantitative practicable scaling method still needs to be figured out.

The above analyses show that it is impractical to carry out the scaling of combustion chamber heat transfer through ensuring Re and Nu constant. Since perfect scaling criterion cannot be obtained for heat transfer, other compromise engineering methods will be employed to obtain the quantitative scaling criterion to avoid the requirement of constant Re condition.

4.2. Specific scaling criterion

Over the past several decades, considerable effort has been dedicated to research on the heat transfer of combustion chambers in LPREs. The most popular methods for calculating the heat flux in combustion chamber are the Yevlev method and Bartz method.

Ievlev obtained the hotgas-wall heat flux calculation method through theoretical analysis and deduction[33,34]

$$\begin{aligned} q &\propto p_c^{*0.87} d_t^{-0.13} M^{0.435} c_p \\ &\times (T^* - T_{wg}) \eta^{0.13} T^{*-0.175} T_{wg}^{-0.26} \\ &= p_c^{*0.87} d_t^{-0.13} S. \end{aligned} \tag{5}$$

In this method, except pressure p_c and throat inner diameter d_t, all other parameters can be ensured constant when the main flowfield is similar. Thus, the heat flux q becomes directly proportional to $p_c^{*0.87} d_t^{-0.13}$.

The Bartz method is a semi-empirical one based on numerous experimental data[34,35]

$$\begin{aligned} q &= \frac{0.026}{d_t^{0.2}} \left(\frac{\eta^{0.2} c_p}{Pr^{0.6}} \right) \left(\frac{p_c^*}{c^*} \right)^{0.8} \left(\frac{A_t}{A} \right)^{0.9} \sigma (T_{ad} - T_{wg}) \\ &= p_c^{*0.8} d_t^{-0.2} S. \end{aligned} \tag{6}$$

Also, when the main flowfields are similar, the heat flux q becomes directly proportional to $p_c^{*0.8} d_t^{-0.2}$.

Ievlev's method comes from theoretical analysis, while Bartz method is semi-empirical based on hot-testing results. Just because they are deduced using different approaches, there is a little difference between them. The following numerical and experimental studies will aim at validating these two quantitative scaling methods respectively for their different applicabilities.

5. Numerical study

Without loss of generality, single-element gas–gas injectors chambers were designed and gaseous oxygen and gaseous hydrogen were chosen as the propellants. The basic injector, a shear-coaxial injector, was selected from the full-scale engine. According to the criterion, the combustion flowfields were calculated in two steps for clearer understanding. first, chamber pressures were kept constant and the chambers had different sizes. Secondly, the sizes were kept constant and the chambers were designed at different pressures. The propellants flowrates changed in both of these two steps.

The basic injector and chamber are shown in Figs. 1 and 2. The design parameters of the chamber are obtained from the full-scale engine. The characteristic length is 800 mm and the contraction ratio is 3.1.

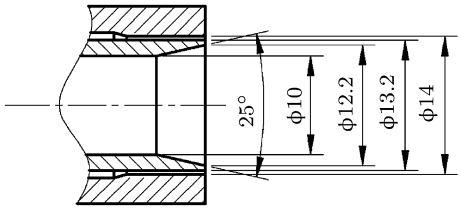


Fig. 1. Schematic diagram of the injectors.



Fig. 2. The calculation domain of the chamber.

5.1. Numerical models

Great effort has been made to perform the computational fluid dynamics (CFD) simulation of gas–gas combustion flow at Pennsylvania State University, NASA Marshall Space Flight Center, University of Michigan and Beihang University etc.[9−11,13,18,20−29] The results indicated that the steady Reynolds average Navier–Stokes (RANS) method combined with a k–ε turbulence model could effectively simulate the whole combustion flow and obtain the statistical average solutions that can match the experimental results. In this study, the RANS method combined with a $k-\varepsilon$ turbulence model was used to compare different conditions in statistical states instead of being used to investigate accurately the transient flowfield solutions. It turned out to be a feasible approach.

Constant pressure specific heat of each species was calculated as a function of temperature

$$C/R = a_0 + a_1T + a_2T^2 + a_3T^3 + a_4T^4 + a_5T^5. \quad (7)$$

In the momentum equations, the transport coefficient $\mu_{\rm eff} = \mu + \mu_{\rm t}$, where $\mu_{\rm t}$ is coefficient of eddy viscosity and $\mu_{\rm t} = \rho C_\mu k^2/\varepsilon$. Coefficients of laminar viscosity and heat conduction of single component were calculated by using molecular dynamics approach. The compressibility of the gas propellants at high pressures was considered. The R–K equation was substituted for the ideal state equation to take the real gas effect into account.

5.2. Numerical method and boundary condition

The entire system was solved by a strongly coupled implicit time-marching method using ADI factorization for the inversion of the implicit operator. Convective terms were 2-order flux split upwinding differenced, whereas diffusion terms were centrally differenced.

The calculation domain occupied only half the chamber. The radial and axial stretchings of the grid were used near the wall boundary and in the shear layer domain. The grid consisted of 29028 cells and the grid of half the cylinder was 43×350.

The inlet fixed mass flowrate and the inlet turbulence intensities were both set to be 5%. The centreline was an axisymmetric boundary and the nozzle exit was specified as a supersonic outlet. Non-slip wall boundaries were used on the chamber walls. The temperature of the combustor wall was set at environment temperature of 300 K to achieve a steady heat flux.

5.3. Geometric scaling

The combustion chamber pressures were kept at the laboratory pressure of 3 MPa in geometric scaling simulations. All lengths of the basic chamber were enlarged by three different universal linear scale factors. A total of 4 cases were chosen and shown in Table 1, which shows that just the scaling conditions of the main flowfield were satisfied, the Re of these cases are different. The combustion flowfields and heat flux along the combustor wall were obtained. The temperature contours are shown in Fig. 3. Based on the heat transfer scaling method Eq. (5), all the heat flux data were scaled by $d_{\rm t}^{-0.13}$ and the results are shown in Fig. 4. The x coordinate $x^* = x/n$, n is the scale factor. It can be seen that all the curves collapse to a single profile, which indicates that the heat fluxes in gas–gas injector combustors of different sizes show a good agreement with Eq. (5). Theoretically, the heat flux data in subscale combustor can be extended to the full scale condition using $q \sim L^{-0.13}$.

Table 1. Parameters of geometric scaling conditions.

Scale factor, n	H_2 flowrate/kg·s^{-1}	H_2 temperature/K	H_2 injection velocity/m·s^{-1}	O_2 flowrate/kg·s^{-1}	O_2 temperature/K	O_2 injection velocity/m·s^{-1}
1	0.0323	300	∼ 760	0.194	300	∼ 70
2	0.1292	300	∼ 760	0.775	300	∼ 70
3	0.2907	300	∼ 760	1.744	300	∼ 70
4	0.5168	300	∼ 760	3.101	300	∼ 70

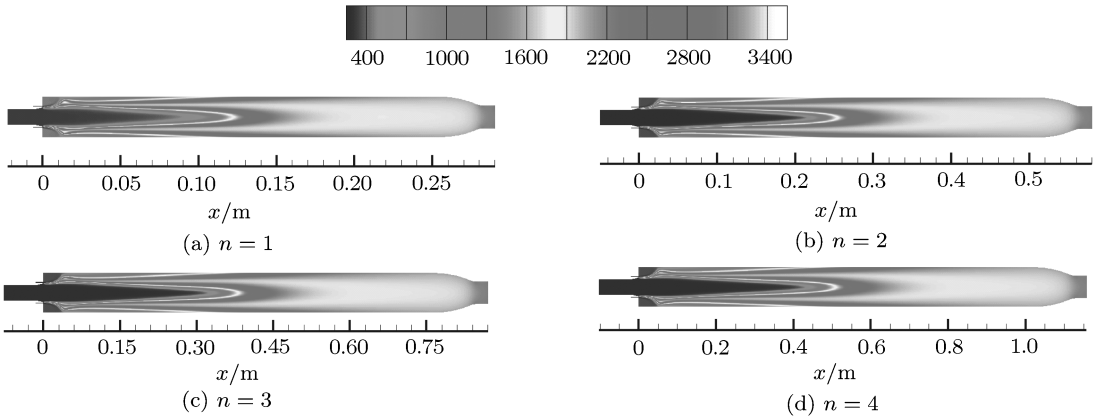


Fig. 3. Temperature contours for four different sizes.

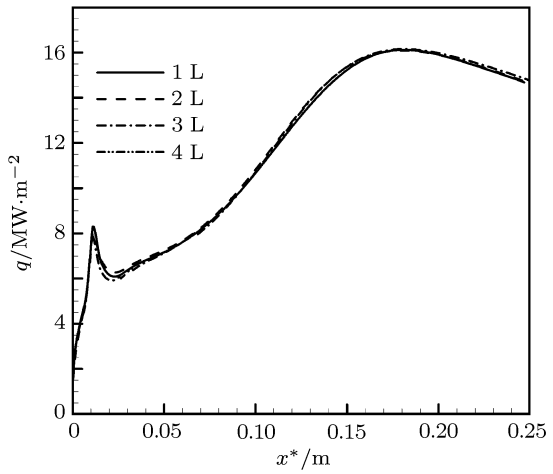


Fig. 4. Heat flux (scaled with respect to $1/n^{-0.13}$) versus axial distance (scaled with respect to $1/n$) for five chamber pressures.

5.4. Pressure scaling

In the calculation of pressure scaling, the dimensions of the chambers were kept unchanged. A total of 5 numerical cases under different pressures were chosen, as shown in Table 2. Also, just the scaling conditions of main flowfield were satisfied, while *Re* of these cases were different. The combustion flowfields and heat flux along with the combustor wall were obtained. The temperature contours are shown in Fig. 5. Based on the heat transfer scaling method in Eq. (5), all the heat flux data are scaled by $p_c^{0.87}$ and the results are shown in Fig. 6. It can be seen that all the curves collapse to a single profile, which indicates that the heat flux in gas–gas injector combustors at different pressures show a good agreement with Eq. (5). Theoretically, the heat flux data in low-pressure combustor can be extended to the high-pressure condition using $q \sim p_c^{0.87}$.

Table 2. Parameters of pressure scaling.

Chamber pressure/MPa	H_2 flowrate/kg·s^{-1}	H_2 temperature/K	H_2 injection velocity/m·s^{-1}	O_2 flowrate /kg·s^{-1}	O_2 temperature/K	O_2 injection velocity/m·s^{-1}
1	0.0108	300	~ 760	0.0648	300	~ 70
5	0.054	300	~ 760	0.324	300	~ 70
10	0.108	300	~ 760	0.648	300	~ 70
15	0.162	300	~ 760	0.972	300	~ 70
20	0.216	300	~ 760	1.296	300	~ 70

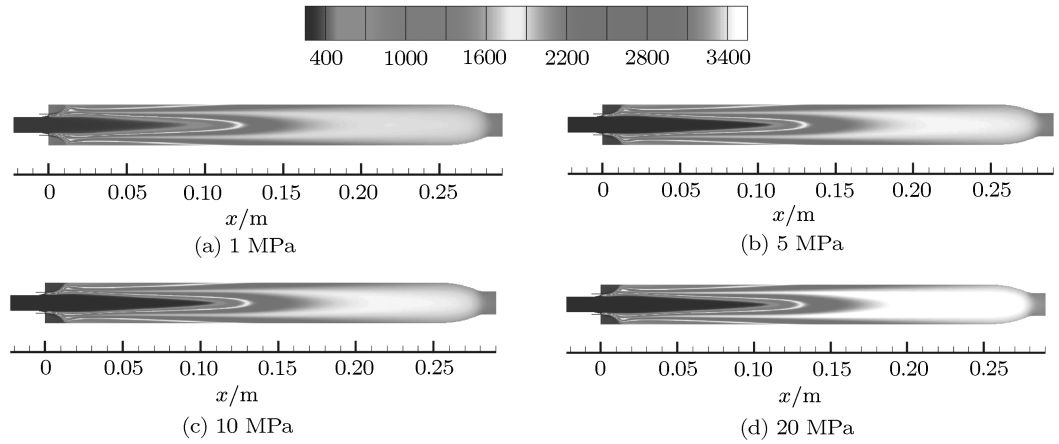


Fig. 5. Temperature contours in the five different pressure cases.

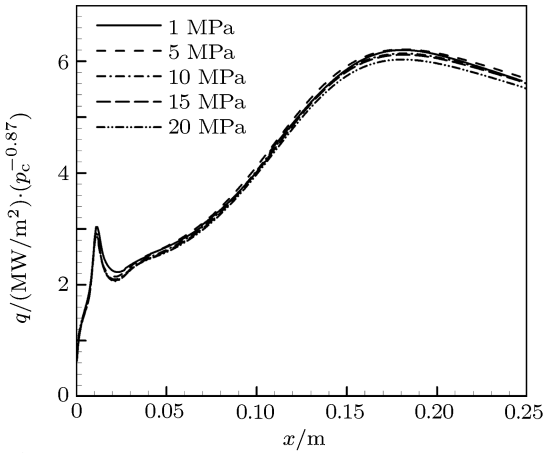


Fig. 6. Heat flux (scaled with respect to $1/p_c^{0.87}$) versus axial distance for five chamber pressure cases.

6. Experimental study

Up to now no experimental study that focuses on the scaling of gas–gas combustion chamber heat transfer has been found. A single-element shear coaxial injector and a combustion chamber were designed, fabricated and hot-fire tested at different chamber pressures in this study. Because the Bartz method is summarized based on experimental data, it is more suitable for hot-testing results. Thus, in this part, Bartz method will be employed.

6.1. Experimental facility and measurement method

The experimental investigation was carried out at the FFSC Laboratory in Beihang University. A simplified schematic of the testing system is shown in Fig. 7.

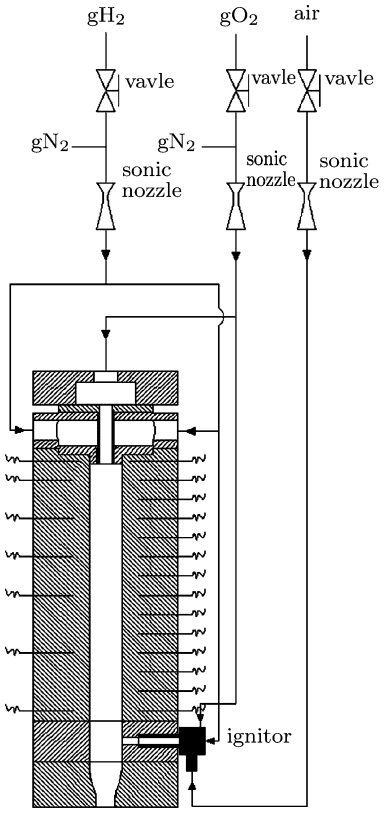


Fig. 7. Facility schematic diagram.

The configuration of the single-element chamber can be seen in Fig. 8. The chamber was modular and could be easily configured to accommodate changes in the injector design and the length or inner diameter of the combustor. The main chamber was a heat-sink design, the cylinder was made of copper and the injector was made of stainless steel. The nozzle was fabricated from ablation resistance material. The cylinder was separated into two parts: the temperature measure-

ment part and the ignition part. The ignitor was a resonance torch one that was heated by air. In pressure scaling tests, the size and configuration of the injector and chamber were designed to be the same as the basic chamber stated in the above numerical analysis part.

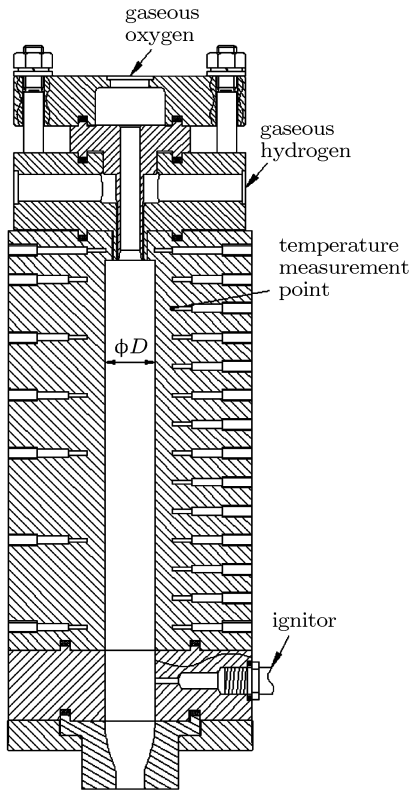


Fig. 8. Schematic diagram of the chamber and thermoscouple locations.

To obtain the inner wall heat flux, a wall temperature measurement method was applied in this study. Some small holes were designed at the locations of the measurement points. The thermocouples measured temperatures at the bottoms of these holes. Axial locations for instrumentation are indicated in Fig. 8. Multiple instrumentations (4 each) were presented at some axial locations and four thermocouples were separated at 90°. The thermocouples used Type-K junctions.

In the pressure scaling tests, because of the heat-sink design of the chamber and the heat protection considered, the durations of the steady hot-fires were set from 1.5 s to 5 s for different chamber pressure cases: 0.92 MPa—5 s, 1.83 MPa—4 s, 2.69 MPa—4 s, 3.63 MPa—3 s, 4.52 MPa—2 s, 5.42 MPa—2 s, 6.1 MPa—1.5 s. And the timing of the tests was designed as follows: The ignitor worked before the injector and once the chamber pressure got steady, the ignitor was shut down.

6.2. Pressure scaling

6.2.1. Test conditions

A total of 17 hot-fire tests were conducted steadily. The operational conditions and typical chamber pressure profiles are summarized in Table 3 and Fig. 9. The nominal MR of all conditions were 6.0, the uncertainties of the MR of tests were -2.8%–2.3%. The parameters shown in Table 3 indicate that all the scaling conditions of the main flowfield were satisfied.

6.2.2. Results and discussion

The time traces of some thermocouples for a representative 2.69 MPa chamber pressure test are shown in Fig. 10. A total of eight sets of thermocouple temperature measurements are shown. In terms of nomenclature in the figure, for example, the first trace labeled TC-10-0° denotes that the thermocouple was at the 10-mm axial location, at 0° degree (angle was defined with respect to major array of thermocouple). Except the curve TC-25-0°, it can be seen that all temperature traces have the same response characteristics, well behave and are not noisy. The TC-25-0° has an obvious longer response time than others, so it cannot be utilized.

Table 3. Test conditions.

Chamber pressure/MPa	OX flowrate/g·s^{-1}	OX temperature/K	Fuel flowrate/g·s^{-1}	Fuel temperature/K	MR	Repeat time
0.92	66.7	∼ 283	11.2	∼ 285	5.96	3
1.83	135.1	∼ 284	22.0	∼ 287	6.14	2
2.69	195.4	∼ 279	32.8	∼ 281	5.95	2
3.63	258.3	∼ 279	44.0	∼ 282	5.87	3
4.52	327.2	∼ 279	54.4	∼ 284	6.01	2
5.42	397.8	∼ 278	65.6	∼ 282	6.06	3
6.1	446.9	∼ 276	76.6	∼ 281	5.83	2

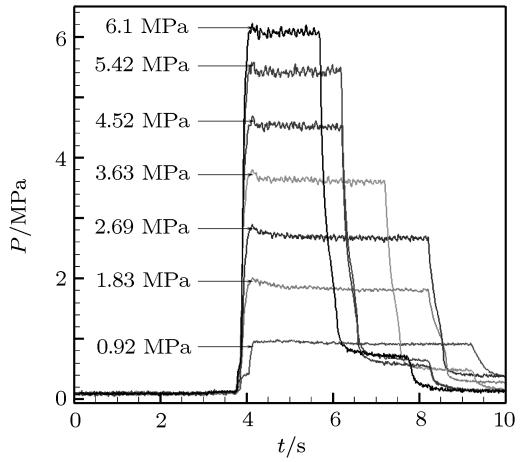


Fig. 9. The typical chamber pressure profiles of 7 cases.

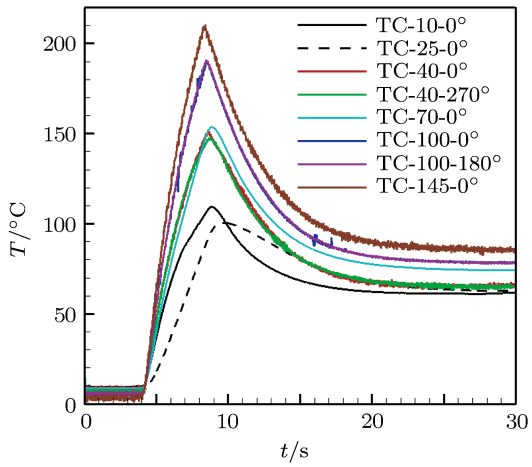


Fig. 10. Thermocouple temperature traces (representative) for a 2.69 MPa test.

During the steady state portion of the firing, the temperatures rose steadily due to the heat sink nature of the chamber design. The curves of two thermocouples located respectively at 40 mm and 100 mm are nearly identical, suggesting that the chamber flow is concentric. According to the theory of heat transfer, higher heat flux on the inner wall at axial location of measurement point consequentially induces higher temperature rise at this point. Picture of the temperature rise at these measurement points versus the axial distance for 2.69-MPa chamber pressure case is shown in Fig. 11, manifesting that the results of 2 repetitive tests are nearly identical.

All temperature curves were obtained for all the pressure cases, then an axisymmetric heat conduction numerical calculation was conducted to obtain the time-averaged hot-gas-wall heat flux for each pressure case. Based on scaling method Eq. (6), all the heat flux data were scaled by $1/p^{0.8}$ and the results are shown in Fig. 12. It can be seen that all the heat flux distribution curves collapse to a single profile and all the cases show the same qualitative distribution trends and almost the same quantitative local values, which means that the heat flux q of a gas–gas injector combustor correlates well with the pressure p as $q \sim p^{0.8}$.

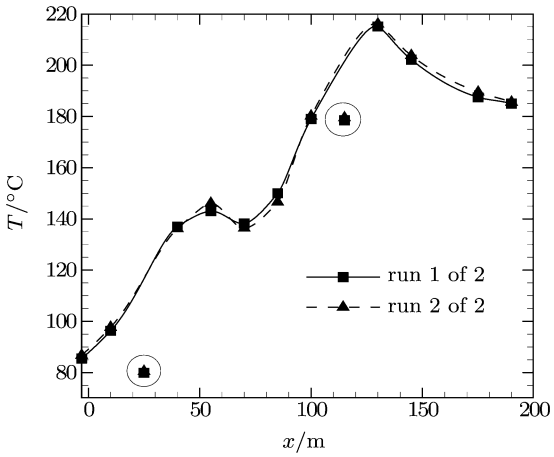


Fig. 11. Wall temperatures versus axial distances for 2.69-MPa chamber pressure case.

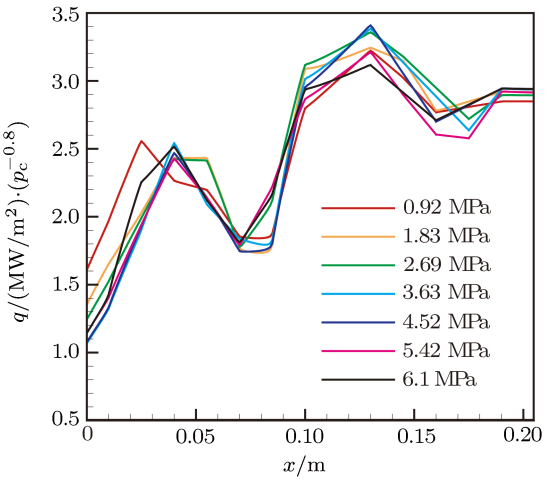


Fig. 12. Heat flux (scaled with respect to $(1/p_c^{0.8})$) versus axial distance for each chamber pressure case.

6.3. Other related experimental study

It was shown in Ref. [15] that in Pennsylvania State University (PSU) a total of 4 chamber pressure condition tests were carried out, of which two propellant combinations each took place in a single-element chamber, to provide the benchmark combustor wall heat flux data for calculation codes. The ambient-temperature gaseous hydrogen and oxygen and the products from oxidizer-rich and fuel-rich preburners

were used respectively. The chamber pressure ranged from 2.07 MPa to 5.18 MPa. In the tests for each propellant combination, the geometries of the injector/chamber were the same, the propellant temperatures, the injection velocities and the wall boundary conditions were not varied. The nominal run conditions are shown in Table 4 and Table 5. These conditions totally accord with the scaling ones of the main flow field and the Re are different for different pressure cases.

In the tests, the combustor inner wall temperature and heat flux were measured and the heat flux versus the axial location of the chamber was obtained for each pressure case. The inner wall heat flux was also scaled with $p^{0.8}$ naturally and tentatively based on the empirical Bartz method by the authors. The results are shown in Figs. 13 and 14.

Table 4. Nominal run conditions for preburner case in Ref. [15].

Chamber pressure p_c/MPa	2.07	3.10	4.14	5.18
H_2 flowrate (fuel preburner)/g·s^{-1}	13.2	19.8	26,4	33
O_2 flowrate (fuel preburner)/g·s^{-1}	36.37	54.56	72.74	90.92
H_2 flowrate (Oxi preburner)/g·s^{-1}	1.09	1.09	1.09	1.09
O_2 flowrate (Oxi preburner)/g·s^{-1}	165	165	165	165
Overall mixture ratio	6.6	6.6	6.6	6.6
Oxidizer injection velocity/m·s^{-1}	142	142	142	142
Fuel injection velocity/m·s^{-1}	795	795	795	795
Velocity ratio	5.6	5.6	5.6	5.6

Table 5. Nominal run conditions for ambient propellant case in Ref. [15].

Chamber pressure p_c/MPa	2.07	3.10	4.14	5.18
H_2 flowrate/g·s^{-1}	7.44	11.16	14.88	18.6
O_2 flowrate/g·s^{-1}	44.64	66.96	89.28	111.6
Mixture ratio	6.0	6.0	6.0	6.0
O_2 injection velocity/m·s^{-1}	77.42	77.42	77.42	77.42
H_2 injection velocity/m·s^{-1}	343	343	343	343
Velocity ratio	4.43	4.43	4.43	4.43

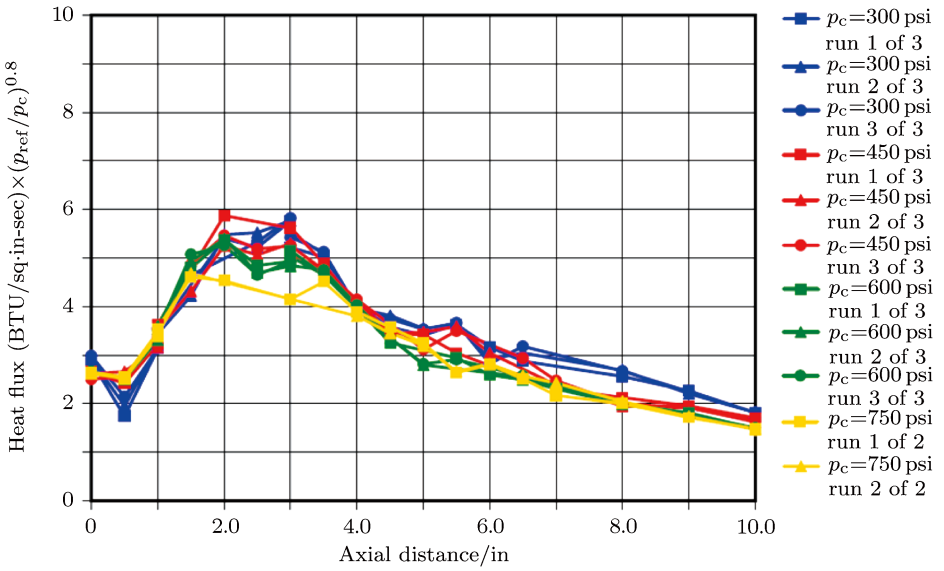


Fig. 13. Heat flux (scaled with respect to (2.07 MPa/p_c)$^{0.8}$) versus axial distance for four chamber pressures (preburner case).[15]

Figures 13 and 14 also show all the heat flux curves at different pressures collapse to a single profile for each propellant combination The same result as that of the experimental study above is obtained. Though the

efforts in Ref. [15] did not aim at the scaling of inner flowfield or heat transfer in a gas–gas injector combustor, its results also validate the theoretical conclusion in this paper.

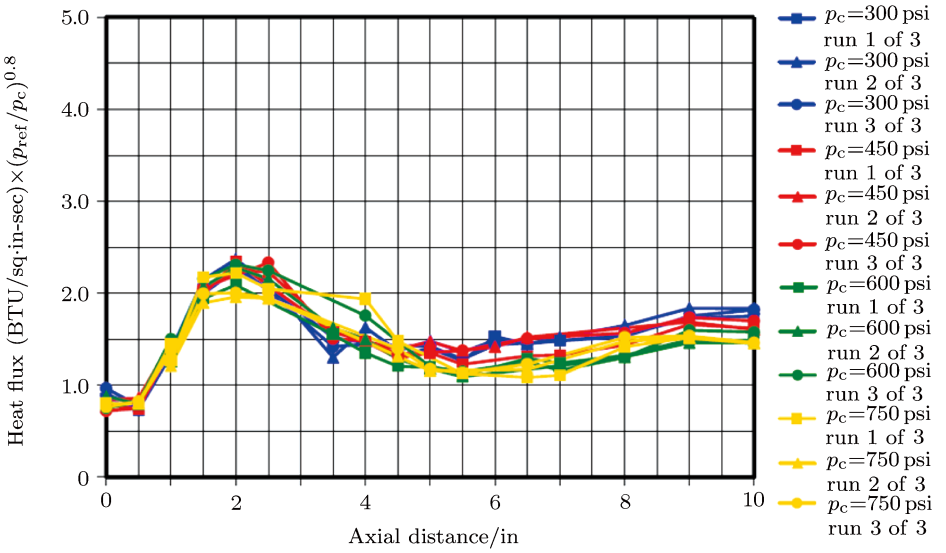


Fig. 14. Heat flux (scaled with respect to (2.07 MPa/p_c)$^{0.8}$) versus axial distance for four chamber pressures (ambient propellant case).[15]

The above study reveals that: in the design and development of a high pressure gas–gas injector combustion chamber, the heat flux of this chamber can be exactly predicted qualitatively and quantitatively by a low-pressure chamber through the relationship $q \sim p^{0.8}$, as long as the simple scaling criterion of inner combustion flowfield is satisfied. This scaling technology can effectively decrease the development cost and period. In addition, in high pressure hot tests for a new injector development, the local exceptional high heat flux always occur, which may lead to dangers. This kind of potential dangers can be avoided effectively by utilising low-pressure hot test to evaluate in advance.

Additionally, one point needs to be explained here. Though the Bartz method has been widely used in the development of LPREs and it also indicates the relationships between heat flux and the design parameters, it is always just used as the initial roughly prediction in practice. For instance, for the traditional gas–liquid mixed combustion engine, the similarity of the whole inner combustion flowfield was found to be practically impossible because of its extreme complexity, thus the qualitative similarity of the heat flux distribution even cannot be obtained at least for gas–liquid combustion engines. Just because of the unique characteristics of gas–gas combustion, which have been analysed in Refs. [27]–[29], the qualitative and quantitative similarity of heat transfer can be obtained in a gas–gas injector combustors.

7. Conclusions

Based on the study on the scaling of gas–gas combustion flowfield, the scaling of gas–gas injector combustor heat transfer was investigated. The similarity condition of the gas–gas injector combustor heat transfer was obtained by conducting a formulation analysis of the gaseous boundary layer Navier–Stokes equations and a dimensional analysis of the corresponding heat transfer phenomenon. The further analysis indicated this perfect similarity condition is impractical. Then a practicable scaling criterion of the gas–gas injector combustor heat transfer was put forward. Numerical and experimental studies of gas–gas injector chambers were carried out to verify the theoretical result. The major conclusions obtained are summarized below.

(I) When the main flowfields are similar, the heat transfer of different gas–gas injector combustors will be prefectly similar as long as Re are kept unchanged. This conclusion is not only suitable for FFSC liquid rocket engine, but also for those engine and combustion devices with gaseous fuels and oxidizers.

(II) As long as the scaling criteria of inner combustion flowfield are satisfied, namely a) the similarity between the geometries of the injector and the chamber; b) identical propellants; c) constant injection ve-

locities and propellant temperatures; d) non-slip and similar species wall boundary; e) flow in laminar or sufficient turbulence conditions, the heat flux distribution along with the combustor wall will be qualitatively similar and any local heat flux is correlated well with the pressure and dimension as $q \propto p_{\rm c}^{0.8} d_{\rm t}^{-0.2}$. The hot-testing data from the low-pressure small-size gas–gas combustion chamber can be exactly extended to high-pressure full-scale chamber, which can greatly decrease the development cost and period or potential dangers.

Acknowledgments

The authors acknowledge the support of the State High-Tech Research and Development Fund and the Innovation Foundation of Beihang University. The authors also thank the Beijing Space Propulsion Experiment Center for the experimental facilities. The authors also thank Zhang W and Li S from Beijing West Zhonghang Technology Ltd. for helps in designing the thermocouples. Finally, the authors thank all the people who made contributions and gave help to this paper.

References

[1] Penner S S 1955 *Combustion Research and Review* AGARD Combustion Colloquium (London: Butterworths) pp. 140–162
[2] Penner S S 1957 *Chemical Problems in Jet Propulsion* (London: Pergamon) pp. 345–347, pp. 376–388
[3] Dexter C E, Fisher M F, Hulka J R, Denisov K P, Shibanov A A and Agarkov A F 2004 *Liquid Rocket Thrust Chambers: Aspects of Modeling, Analysis and Design* ed. Yang V, Habiballah M, Hulka J, and Popp M, in *Progress in Astronautics and Aeronautics* **200** 553
[4] Kenny R J, Moser M D, Hulka J R and Jones G 2006 *AIAA Paper* 2006–4705
[5] Hulka J R 2008 *AIAA Paper* 2008–5113
[6] Davis J A and Campbell R L 1997 *AIAA Paper* 1997–3118
[7] Wim A de Groot, Thomas J McGuire and Steven J Schneider 1997 *AIAA Paper* 1997–2847
[8] Calhoon D, Ito J and Kors D 1973 *NASA CR*-121234, Contract NAS3–13379
[9] Foust M J, Deshpande M, Pal S, Ni T, Merkle C L and Santoro R J 1996 *AIAA Paper* 1996–0646
[10] Schley C A, Hagemann G and Tucker P K 1997 *AIAA Paper* 1997–3302
[11] Tucker P K, Klemt M D and Smith T D 1997 *AIAA Paper* 1997–3350
[12] Farhangi S, Yu T, Rojas L, Sprouse K and McKinnon J 1999 *AIAA Paper* 1999–2757
[13] Archambault M R, Talley D and Peroomian O 2002 *AIAA Paper* 2002–1088
[14] Smith T D, Klem M D and Breisacher K J 2002 *NASA/TM*-2002–211982
[15] Marshall W M, Pal S, Woodward R D and Santoro R J 2005 *AIAA Paper* 2005–3572
[16] Lin J, West J S, Williamst R W, Tucker P K and Chenoweth J D 2005 *AIAA Paper* 2005–4524
[17] Tucker P K, Menon S, Merkle C L, Oefelein J C and Yang V 2007 *AIAA Paper* 2007–5572
[18] Tucker P K, Menon S, Merkle C L, Oefelein J C and Yang V 2008 *AIAA Paper* 2008–5226
[19] Vaidyanathan R, Tucker P K, Papial N and Shyy W 2004 *J. Propul. Power* **20** 705
[20] Sozer E, Vaidyanathan A, Segal C and Shyy W 2009 *AIAA Paper* 2009–449
[21] Cai G B, Wang X W, Jin P and Gao Y S 2008 *AIAA Paper* 2008–4562
[22] Wang X W, Cai G B and Gao Y S 2009 *AIAA Paper* 2009–5042
[23] Wang X W, Gao Y S and Cai G B 2010 *J. Aerospace Power* **35** (in Chinese)
[24] Wang X W, Gao Y S and Cai G B 2010 *J. Aerospace Power* **35** (in Chinese)
[25] Wang X W, Jin P, Zhang G Z and Cai G B 2008 *J. Propulsion Technology* **4** 407 (in Chinese)
[26] Wang X W, Jin P and Cai G B 2009 *J. Beijing University of Aeronautics and Astronautics* **35** (in Chinese)
[27] Wang X W, Jin P and Cai G B 2010 *Acta Aeronautica et Astronautica Sinica* **32** 1305 (in Chinese)
[28] Cai G B, Wang X W, Jin P and Gao Y S 2011 *J. Propulsion and Power* (accepted)
[29] Wang X W, Cai G B and Jin P 2010 *Chin. Phys.* B **19** 019401
[30] Gao Y W 2002 *Experimental Fluid Dynamics* (Xi'an: Northwestern Polytechnical University Press)
[31] Pope S B 2000 *Turbulent Flows* (Cambridge: Cambridge University Press)
[32] Bian B M, He A Z, Li Z H, Yang L, Zhang P, Shen Z H and Ni X W 2005 *Acta Phys. Sin.* **54** 5534 (in Chinese)
[33] Ievlev V M 1953 *Rocket Engines* (Moscow: National Defence Industry Press) (in Russion)
[34] Liu G Q 1993 *Theory of Rocket Engines* (Beijing: Aerospace Press)
[35] Bartz D R 1968 in *Advances in Rocket Propulsion* ed. Penner S S (Manchester: AGARD, Technivision Services)